

# Graphite-Supported Pt<sub>n</sub> Cluster Electrocatalysts: Major Change of Active Sites as a Function of the Applied Potential

Julen Munarriz, Zisheng Zhang, Philippe Sautet,\* and Anastassia N. Alexandrova\*



Cite This: ACS Catal. 2022, 12, 14517–14526



Read Online

ACCESS |

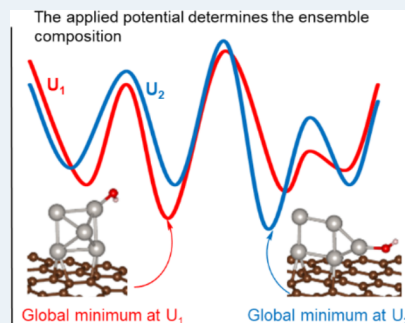
Metrics & More

Article Recommendations

Supporting Information

**ABSTRACT:** The oxygen reduction reaction (ORR) plays a key role in renewable energy transformation processes. Unfortunately, it is inherently sluggish, which greatly limits its industrial application. Sub-nano-cluster-decorated electrode interfaces are promising candidate ORR electrocatalysts. However, understanding the nature of the active sites on these catalysts under electrocatalytic conditions presents a formidable challenge for both experiment and theory, due to their dynamic fluxional character. Here, we combine global optimization with the electronic Grand Canonical DFT to elucidate the structure and dynamics of subnano Pt<sub>n</sub> clusters deposited on electrified graphite. We show that, under electrochemical conditions, these clusters exist as statistical ensembles of multiple states, whose fluxionality is greatly affected by the applied potential, electrolyte, and adsorbate coverage. The results reveal the presence of potential-dependent active sites and, hence, reaction energetics.

**KEYWORDS:** Cluster catalysis, Electrochemistry, Fluxionality, Oxygen Reduction Reaction, DFT



## INTRODUCTION

The progressive fossil fuels depletion in conjunction with the need for reducing environmental pollution has motivated an increasing interest in the search for renewable and efficient energy processes.<sup>1</sup> Electrocatalysis plays a crucial role in this field, as it is at the heart of many state-of-the art energy technologies such as fuel cells,<sup>2</sup> hydrogen producing devices,<sup>3</sup> and photovoltaic systems.<sup>4</sup> In this context, (subnano) Pt-based clusters are promising catalysts for important electrocatalytic processes such as the Oxygen Reduction Reaction (ORR).<sup>5–10</sup> However, they are complex systems, which exhibit many intriguing features that make their study a challenge. Namely, the activity and selectivity of size-selected Pt<sub>n</sub> ( $n = 1–14$ ) clusters deposited on glassy carbon and indium tin oxide depend strongly and nonmonotonically on the cluster size.<sup>11–15</sup> Moreover, one key feature of size-selected supported Pt<sub>n</sub> clusters is their high fluxional character, which leads to various competing low energy structures. This results in their capability to change shape from thermal fluctuations and in response to the number and nature of the adsorbates. One consequence is that they can circumvent the generally accepted scaling relations of ORR.<sup>16–18</sup>

In electrochemical processes, the catalytic interface can be highly impacted by the applied potential. For example, Reuter and co-workers showed from first-principles that the electrode potential causes reconstruction of IrO<sub>2</sub> nanoparticles,<sup>19</sup> and Roldan et al. showed a significant restructuring of Cu nanoparticles under CO<sub>2</sub> electro-reduction conditions.<sup>20</sup> Many catalytic intermediates also exhibit potential-dependent coordination modes, such as pyridine on Au(111),<sup>21</sup> oxalate on

Ni(111),<sup>22</sup> and activated CO<sub>2</sub> on Cu(211).<sup>23</sup> These observations, in conjunction with the high fluxionality, and structural sensitivity of Pt clusters to the reaction conditions,<sup>24</sup> are suggestive of (a) several structures and hence active sites present under given electrochemical conditions and (b) a strong dependence of these available active site(s) on the electrochemical conditions on a cluster-decorated interface.

Notice that, at an electrochemical interface, the number of electrons is not fixed, as the electrode acts as a source (cathode) or sink (anode) of electrons. Instead, it is the electrochemical potential that stays constant throughout the chemical reaction. Also, sub-nano-clusters are, as other molecular systems, known to adopt different shapes in their different charge state (cationic, neutral, or anionic). Thus, we expect that the explicitly included electrochemical potential should produce significant alterations of the cluster-decorated electrocatalytic interface, as pointed out by some of us in a recent exploratory work.<sup>25</sup> This way, the central goal of this study is the elucidation of the structural evolution, reagent coverage, and resultant ORR activity of sub-nano-Pt clusters deposited on carbon-based electrodes, in the presence of an applied potential and for various adsorbate coverages.

Received: September 20, 2022

Revised: October 30, 2022

Published: November 11, 2022



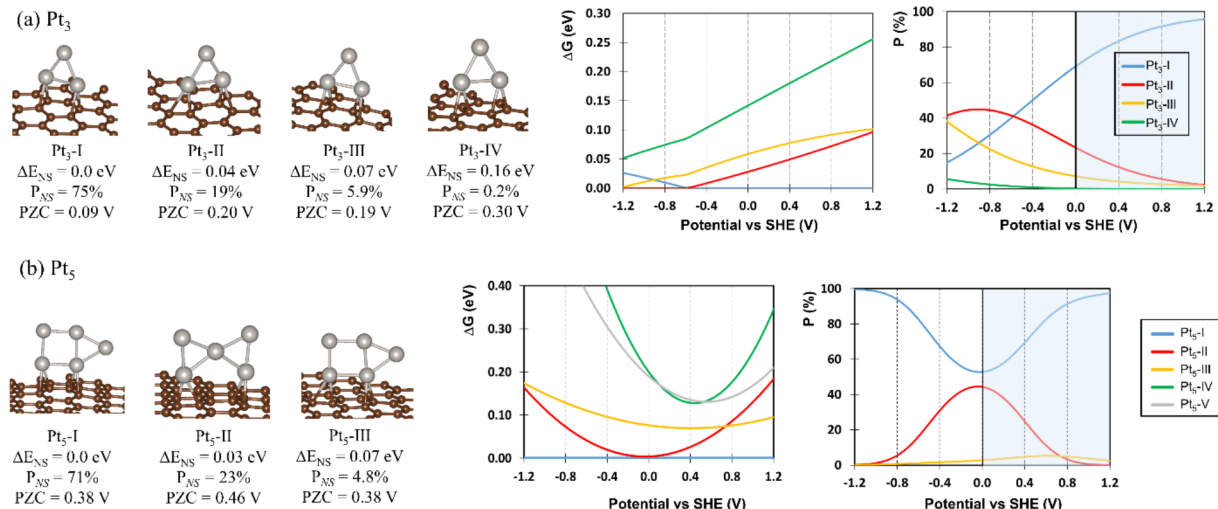


**Figure 1.** Left: Selected local minima, relative energy with respect to the GM for the neutral systems ( $\Delta E_{NS}$ ), PZC, and Boltzmann cluster populations at 300 K considering the neutral systems ( $P_{NS}$ ). Right:  $\Delta G$  (with respect to the GM at each potential) as a function of the potential (with regard to SHE), and Boltzmann cluster distribution as a function of the potential at 300 K in the SC framework for (a) Pt<sub>3</sub> and (b) Pt<sub>5</sub> systems. The more realistic potential range 0.0–1.2 V is highlighted in light blue.

The methodology suitable for this task requires a special note. While previous studies addressed ORR on graphite/graphene supported Pt clusters,<sup>26–30</sup> the global optimization typically required for small clusters has rarely been accomplished under electrochemical conditions. At this point, we should comment on the work of Nakajima and co-workers, who have studied graphite-based surfaces decorated with Pt<sub>n</sub> clusters by preoptimizing the clusters in the gas phase and then depositing them on the surface, the potential effect being later included by means of the Computational Hydrogen Electrode (see below). In order to identify the relevant clusters under working conditions, they relied on XAFS spectroscopy and used it to match the observations with some of the DFT computed structures.<sup>15,31</sup> Even though their approach is, without any doubt, valuable, they had to recur to experimental evidence to identify the global minimum (GM) and did not consider ensemble effects. In this sense, our perspective is different, as it is enforced to extract the chemical information from simulations without requiring external input.

Indeed, accounting for the potential-dependent effects in adsorption and especially fluxionality is not trivial and cannot be done, for example, within the widely used Computational Hydrogen Electrode (CHE) model.<sup>32</sup> In this work, we therefore combine global optimization techniques with an explicit grand canonical modeling of the electrochemical potential, which employs the surface charging (SC) technique combined with the linearized Poisson–Boltzmann (PB) implicit solvation model as reported in ref 21. Adding full explicit solvation and the sufficient statistical mechanical sampling of the solvent and ions to the scheme would be prohibitively expensive.<sup>33</sup> Therefore, we resort to implicit solvation with the PB model of the electrolyte<sup>34</sup>—the approach has demonstrated success for a variety of electrochemical processes.<sup>21,35,36</sup> We note that some authors have reported that linearized Poisson–Boltzmann models cannot provide a fully satisfactory description of electrolyte–electrode interfaces.<sup>37</sup> Nonetheless, our main focus is on the geometry of Pt<sub>n</sub> clusters and its dependence on the applied potential, rather than on the specific electrolyte–electrode interaction, and we expect that the conclusions extracted from this work will hold

when applying more elaborate electrochemical models. In this regard, we highlight that modeling the electrochemical reconstruction of interfaces is very challenging, and new theoretical methods continue to be developed.<sup>37–45</sup>

We studied the effect of the applied potential on the ensemble composition of Pt<sub>n</sub> ( $n = 3, 5$ ) size-selected sub-nano-clusters deposited over graphite and in the presence of relevant intermediates of ORR (for Pt<sub>5</sub> systems). We selected graphite as a model system for the support, which is generally based on amorphous carbon-based structures, an approach that has been applied by us, as well as other authors (either using graphite or graphene).<sup>15,16,25</sup> Herein, we do not address the effect of the Pt–support interaction in heterogeneous supports due to computational limitations, which has been addressed by other authors;<sup>46–50</sup> nonetheless, we expect our main conclusions to qualitatively hold independently of the support. We note that some recent works have computationally studied the potential dissolution of Pt clusters in acidic environments,<sup>51</sup> as well as sintering effects,<sup>52</sup> and the stability of other electrocatalytic systems under different electrocatalytic conditions.<sup>53</sup> We also highlight that monodisperse ensembles of Pt clusters adsorbed on a variety of surfaces have been experimentally prepared and are therefore worth exploring to better understand such systems,<sup>5,6,11–15</sup> without prejudice to the analysis of the aforementioned effects, which, although worth exploring, are out of the scope of this work—in which we aim to analyze cluster fluxionality as a function of the applied potential.

Overall, we believe our approach is innovative and can offer a significant advance in the understanding of dynamic electrochemical catalytic interfaces.

## RESULTS AND DISCUSSION

The structures for the global optimizations were generated by our in-house code, PGOPT, with a bond length distribution algorithm (BLDA),<sup>54</sup> and optimized with dispersion-corrected DFT in the presence of an electrostatic potential (with respect to the standard hydrogen electrode),  $U(\text{SHE})$ . We selected an electrolyte concentration of 1 M and analyzed the electrochemical potential in the 0–1.2 V range. We start with the potential dependence of bare clusters, the presence of

adsorbates being presented later. This is a purely theoretical view, since clusters will be adsorbate covered at many potential values. At negative potentials, they are expected to be covered by hydrogen, and a hydrogen evolution reaction will take place. Hydrogen coverage is also expected at small positive potentials due to well-known hydrogen underpotential deposition, which is a consequence of a strong interaction between hydrogen and the Pt in the cluster.<sup>55,56</sup> Nonetheless, the analysis in the full (hypothetical) range allows gauging a baseline of the possible extent of cluster fluxionality under the applied potential, and we expect these baseline dynamics to affect the system behavior in the presence of relevant adsorbates. A full description of the computational details is provided in the Supporting Information.

**Pt<sub>1</sub> and Pt<sub>2</sub> Clusters.** Pt<sub>1</sub> and Pt<sub>2</sub> clusters over a graphite surface are considered first. All of the initial structures of Pt<sub>1</sub> converged to the same minimum, in which Pt is in the bridging position over a single C–C bond (Figure S1a). This adsorption mode has been reported by other authors.<sup>26,57</sup> For Pt<sub>2</sub> structures, we also found a single predominant coordination mode, in which the Pt atoms lie over two C–C bonds belonging to adjacent hexagonal rings (Figure S1b). The predicted potential dependence of these structures is minimal.

**Pt<sub>3</sub> Clusters.** Pt<sub>3</sub> clusters have a more diverse conformational distribution: Five different local minima were found within the energy cutoff with respect to the GM of 0.7 eV, when no applied potential is included. The energy cutoff was chosen generously to account for the possible differential (de)stabilization of the isomers when the potential is applied. The various structures are labeled as Pt<sub>3</sub>-#min, where #min indicates the stability order with respect to the GM when the potential effect is not considered (neutral system), and this nomenclature is kept for the following systems.

All of the structures are Pt triangles, whose dimensions and adsorption sites on the support differ slightly (Figure 1a). The four most stable structures are within less than 0.2 eV from the GM. Pt<sub>3</sub>-V is significantly less stable than the other isomers, and, even when the potential effect is considered, it does not contribute to the overall Boltzmann ensemble at room temperature.

Isomers Pt<sub>3</sub>-I–Pt<sub>3</sub>-IV exhibit sensitivity and order switching as a function of the applied potential. Note that, under CHE, the energy difference between the minima would be constant (and equal to that of the neutral system), and their statistical distribution would not change as a function of the potential. This way, the Boltzmann structural ensemble at 300 K would consist of 75% of Pt<sub>3</sub>-I, 19% of Pt<sub>3</sub>-II, and so on; see  $P_{\text{NS}}$  entry in Figure 1— $P_{\text{NS}}$  corresponds to the Boltzmann probability when taking the energy results for the neutral systems, which is the basis of the CHE model. In contrast, when we explicitly account for the potential via SC, the picture changes dramatically. For example, the distribution of Pt<sub>3</sub>-I now varies as a function of the potential, between 15 and 96% at 300 K, which is a typical temperature in electrocatalysis (see Figure 1). We note that the ability to fully rearrange into an equilibrium thermodynamic ensemble in response to the current conditions is assumed in this study. Such an assumption is supported by previous theoretical and experimental findings.<sup>58,59</sup> Namely, some of us proposed on the basis of theoretical calculations (DFT in conjunction with GO and molecular dynamics simulations) that Pt<sub>7</sub> clusters deposited over Al<sub>2</sub>O<sub>3</sub> can very rapidly interconvert.<sup>58</sup> Moreover, interconversion between several isomers of Pt<sub>4</sub> clusters in

a graphene-based support has been experimentally detected.<sup>59</sup> Nonetheless, we acknowledge that the generality of this assumption should be investigated in the future, including in the experiment, and that the change in the potential might lead to metastable clusters that are kinetically trapped at some potentials, which could be relevant for the catalysis.

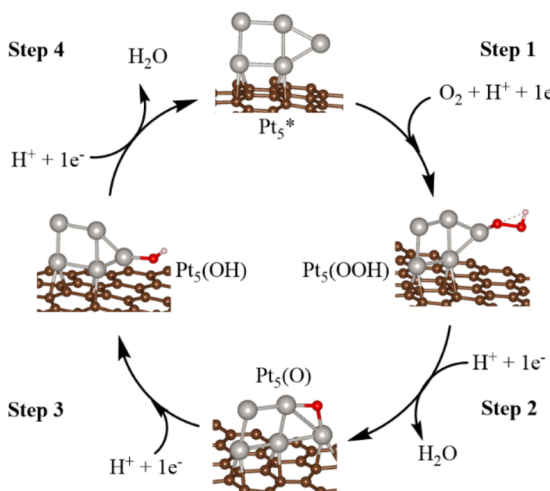
Remarkably, a potential-dependent switch in the GM, between Pt<sub>3</sub>-I and Pt<sub>3</sub>-II, is observed at -0.6 V. Even though at  $U(\text{SHE}) > -0.6$  V the GM remains unchanged (as Pt<sub>3</sub>-I), the 300 K populations of various isomers (Pt<sub>3</sub>-I to Pt<sub>3</sub>-III) change as a function of  $U(\text{SHE})$  (Figure 1a). In fact, no isomer is fully predominant at any potential, and the ensemble composition can be modified by switching the potential. For example, at 0.3 V the ensemble contains 80% of Pt<sub>3</sub>-I, 15% of Pt<sub>3</sub>-II, and 5% of Pt<sub>3</sub>-III. While in this case the structures are relatively similar, these results are relevant, as they show the important effect of the applied potential in governing the cluster probability distribution.

This GM switch is, in broad strokes, a consequence of the potential of zero charge (PZC) difference between the various isomers (i.e., 0.09 V for Pt<sub>3</sub>-I and 0.20 V or Pt<sub>3</sub>-II), which determines the center of the parabolic dependence of the cluster Gibbs energy with respect to the potential, as the parabola's curvature (related to the system polarizability, Figure S3) is qualitatively similar. Note that PZC corresponds to the potential at which the free energy potential parabola has zero first order derivatives with respect to the potential, that is, the location of the maximum. The PZC changes even further for larger and more geometrically diverse clusters (*vide infra*). This difference in the cluster behavior as a function of the potential has been attributed to the differences in the surface dipole moments, which naturally change when the cluster shape changes.<sup>21</sup>

**Pt<sub>5</sub> Clusters.** The Pt<sub>4</sub>/graphite system was addressed in a recent separate study.<sup>25</sup> Pt<sub>5</sub> clusters show a growing geometric diversity (Figure 1b and Figure S4). Pt<sub>5</sub>-I (and also Pt<sub>5</sub>-III) exhibits a distorted pentagonal geometry, which has previously been attributed to a second order Jahn–Teller effect,<sup>60</sup> hinting at the sensitivity of its stability to the electron count. Indeed, the populations for Pt<sub>5</sub>-I and Pt<sub>5</sub>-II range between 53 and 100% and 0.1–44%, respectively, at 300 K (Figure 1b), following the large variations in the energy gap between these structures with the change of the potential. For instance, at 0.0 V, when Pt<sub>5</sub>-II is stabilized the most, it is less than 0.01 eV above Pt<sub>5</sub>-I, which corresponds to 44% of Pt<sub>5</sub>-II and 53% of Pt<sub>5</sub>-I at 300 K. Note that there is a region of the potential of a significant coexistence of Pt<sub>5</sub>-I, Pt<sub>5</sub>-II, and Pt<sub>5</sub>-III (at 300 K) at about 0.7 V. It might seem surprising that Pt<sub>5</sub>-I is stabilized at both more positive and more negative potentials. As shown in Figure S5, it is a consequence of the very different curvature of the Gibbs energy vs potential parabolic fitting, which is much higher for Pt<sub>5</sub>-I. Within the CHE model, the populations would stay constant, at 71% of Pt<sub>5</sub>-I and 23% of Pt<sub>5</sub>-II.

**Potential- and Coverage-Dependent ORR Energetics on Pt<sub>5</sub>/Graphite.** We now focus on the largest cluster considered in this study, Pt<sub>5</sub>/graphite, and report on the impact of the potential and adsorbate coverage effects on the ORR activity. First, we study the adsorption of the reaction intermediates for the four-electron ORR mechanism (Scheme 1), \*O, \*OH, and \*OOH.<sup>61</sup> Note that adsorption can be coupled to geometric rearrangements of the cluster, beyond simple relaxation, leading to the reagent itself preparing the

**Scheme 1. Schematic Representation of the Four-Electron Mechanism of ORR<sup>a</sup>**



<sup>a</sup>A model Pt<sub>5</sub> cluster with a single adsorbate has been taken as reference for visual purposes.

real active site possibly absent on the bare catalyst.<sup>16,62–64</sup> Hence, we aim to interrogate how the nature of the active sites changes as a function of the nature and coverage of the bound intermediates, as well as the applied potential, simultaneously.

**Pt<sub>5</sub> Clusters with One Adsorbate.** Adding one adsorbate dramatically affects the structural morphology of Pt<sub>5</sub>/graphite. Importantly, the cluster geometry is also potential-dependent (Figure 2a–c). For all three considered adsorbates, \*OH, \*O, and \*OOH, the ensemble at 300 K is composed mainly of two different cluster isomers, with potential-dependent proportions.

For Pt<sub>5</sub>(OH) clusters, we found a potential-dependent GM: Pt<sub>5</sub>(OH)-I or Pt<sub>5</sub>(OH)-IV. Although the neutral Pt<sub>5</sub>(OH)-IV is 0.28 eV above the GM (being the fourth most stable geometry), PZCs for Pt<sub>5</sub>(OH)-I and Pt<sub>5</sub>(OH)-IV are significantly different (0.31 and 0.11 V, respectively), and the curvatures in the parabola are also different (Figure S7). As a result, Pt<sub>5</sub>(OH)-IV becomes dominant at 1.1 V. On the contrary, neutral system results (CHE model) would lead to 99% of Pt<sub>5</sub>(OH)-I, 1% of Pt<sub>5</sub>(OH)-II, and no relevant proportions of Pt<sub>5</sub>(OH)-IV (at 300 K).

For Pt<sub>5</sub>O clusters, two structures (Pt<sub>5</sub>O-I and Pt<sub>5</sub>O-II, Figure 2) are very close in energy, with an energy difference of 0.04 eV for the neutral systems, corresponding to 85% of Pt<sub>5</sub>O-I and 15% of Pt<sub>5</sub>O-II at 300 K. Importantly, the SC modeling of the potential induces two switches in the GM, alternating between these two structures (see Figure 2b). The double switch is a consequence of the parabolic shape of the Gibbs energy with the potential, which in this case translates into Pt<sub>5</sub>O-I being predominant in the 0.1–0.8 V range, and Pt<sub>5</sub>O-II outside of this range. This behavior is attributed to the significantly different values of PZC, but especially to the very different parabola curvature (i.e., in the capacitance variation of these clusters), which is much more pronounced for Pt<sub>5</sub>O-I (see Figure S9).

The same behavior of alternation between two structures is obtained for Pt<sub>5</sub>(OOH) clusters, with two minima, Pt<sub>5</sub>(OOH)-I and Pt<sub>5</sub>(OOH)-II (Figure 2c), that are only 0.07 eV apart when the potential effect is not taken into account. This energy difference would correspond to 94% of Pt<sub>5</sub>(OOH)-I and 6% of

Pt<sub>5</sub>(OOH)-II at 300 K. Inclusion of the potential via SC changes the picture: in the 0.0–1.2 V range, the Pt<sub>5</sub>(OOH)-I population varies from 0.1% to 94% (reaching the maximum at ca. 0.4 V) and that of Pt<sub>5</sub>(OOH)-II ranges between 6 and 100% (reached at ca. 1.1 V, see Figure 2). There is a GM switch from Pt<sub>5</sub>(OOH)-I to Pt<sub>5</sub>(OOH)-II at ca. 0.8 V—again a consequence of the very different parabola curvatures (see Figure S11).

**Pt<sub>5</sub> Clusters with Two Adsorbates.** Interestingly, additional adsorbates change the GM, and that is especially significant for Pt<sub>5</sub>(OH)<sub>2</sub> and Pt<sub>5</sub>(OOH)<sub>2</sub> (Figure 2d and f), whose geometrical structures are completely different from those of Pt<sub>5</sub>(OOH) and Pt<sub>5</sub>(OH). For OH, the preferred binding mode changes from atop to bridge. Contrarily to the previous case, the GM is constant in the entire potential range: 100% of Pt<sub>5</sub>(O)<sub>2</sub> is in Pt<sub>5</sub>(O)<sub>2</sub>-I (Figure 2e), and 96–100% of Pt<sub>5</sub>(OOH)<sub>2</sub> is in Pt<sub>5</sub>(OOH)<sub>2</sub>-I (Figure 2f). The collapse of the ensemble to a single structure is a signature of particular stability, reached through adsorbate induced geometric change, and making the adsorption stronger.<sup>65</sup> The potential-dependent geometric variation is somewhat more pronounced for Pt<sub>5</sub>(OH)<sub>2</sub>, where the population of GM, Pt<sub>5</sub>(OH)<sub>2</sub>-I, oscillates between 85 and 100% (Figure 2d). Due to lower structural variation with the potential, the results in this case would be closer to those of the CHE model, which predicts populations of Pt<sub>5</sub>(OOH)<sub>2</sub>-I, Pt<sub>5</sub>(O)<sub>2</sub>-I, and Pt<sub>5</sub>(OH)<sub>2</sub>-I of 92%, 100%, and 96% at 300 K. Notice also that modeling these catalysts under insufficient coverage apparently can lead to a misrepresentation of the active site.

**Pt<sub>5</sub> Clusters with Three, Four, and Five OH Adsorbates.** As will be shown below, the analysis of the ORR energetics reveals the fourth step (protonation of \*OH to yield water) to be thermodynamically limiting. This is because the \*OH binding is the most exothermic for one and two adsorbates (Figure 3), which would lead to the clusters at the catalytic interface being covered by the \*OH adsorbates.<sup>61</sup> Hence, we focus on \*OH and increase the adsorbate coverage. The third \*OH adsorbate reinvigorates the potential dependence of the GM (Figure 2g). For the neutral systems, Pt<sub>5</sub>(OH)<sub>3</sub>-I is 0.20 eV more stable than Pt<sub>5</sub>(OH)<sub>3</sub>-II, which corresponds to relative proportions of 99.9 and 0.05%, respectively, at 300 K. However, in the more elaborate SC framework, GM switches at 0.9 V from Pt<sub>5</sub>(OH)<sub>3</sub>-I (structurally related to Pt<sub>5</sub>(OH)<sub>2</sub>-I) to Pt<sub>5</sub>(OH)<sub>3</sub>-II. Contrarily to other cases, in which GM switches were associated with significantly different PZCs, in this case the two structures have very similar values of PZC: 0.32 and 0.28 V, respectively. Nonetheless, the capacitances are very different, as revealed by a significantly higher curvature in the parabola for Pt<sub>5</sub>(OH)<sub>3</sub>-II (see Figure S16), which is responsible for it being more stable from 0.9 V on.

The addition of a fourth \*OH adsorbate also brings important consequences for the ensemble composition. GM changes three times as a function of the potential in the studied widow (Figure 2h). The GM for the neutral systems, Pt<sub>5</sub>(OH)<sub>4</sub>-I, is predominant in the 0.25–1.1 V range, Pt<sub>5</sub>(OH)<sub>4</sub>-II is GM up to 0.25 V, and Pt<sub>5</sub>(OH)<sub>4</sub>-IV is GM at potentials above 1.1 V. Notice that the structural diversity of cluster geometry is reflected in the electrochemical behavior; namely, PZC varies in a wide range: 0.27 V for Pt<sub>5</sub>(OH)<sub>4</sub>-I, 0.50 V for Pt<sub>5</sub>(OH)<sub>4</sub>-II, 0.34 V for Pt<sub>5</sub>(OH)<sub>4</sub>-III, and 0.14 V for Pt<sub>5</sub>(OH)<sub>4</sub>-IV. This, in conjunction with different parabola curvatures (Figure S18), results in the aforementioned stability

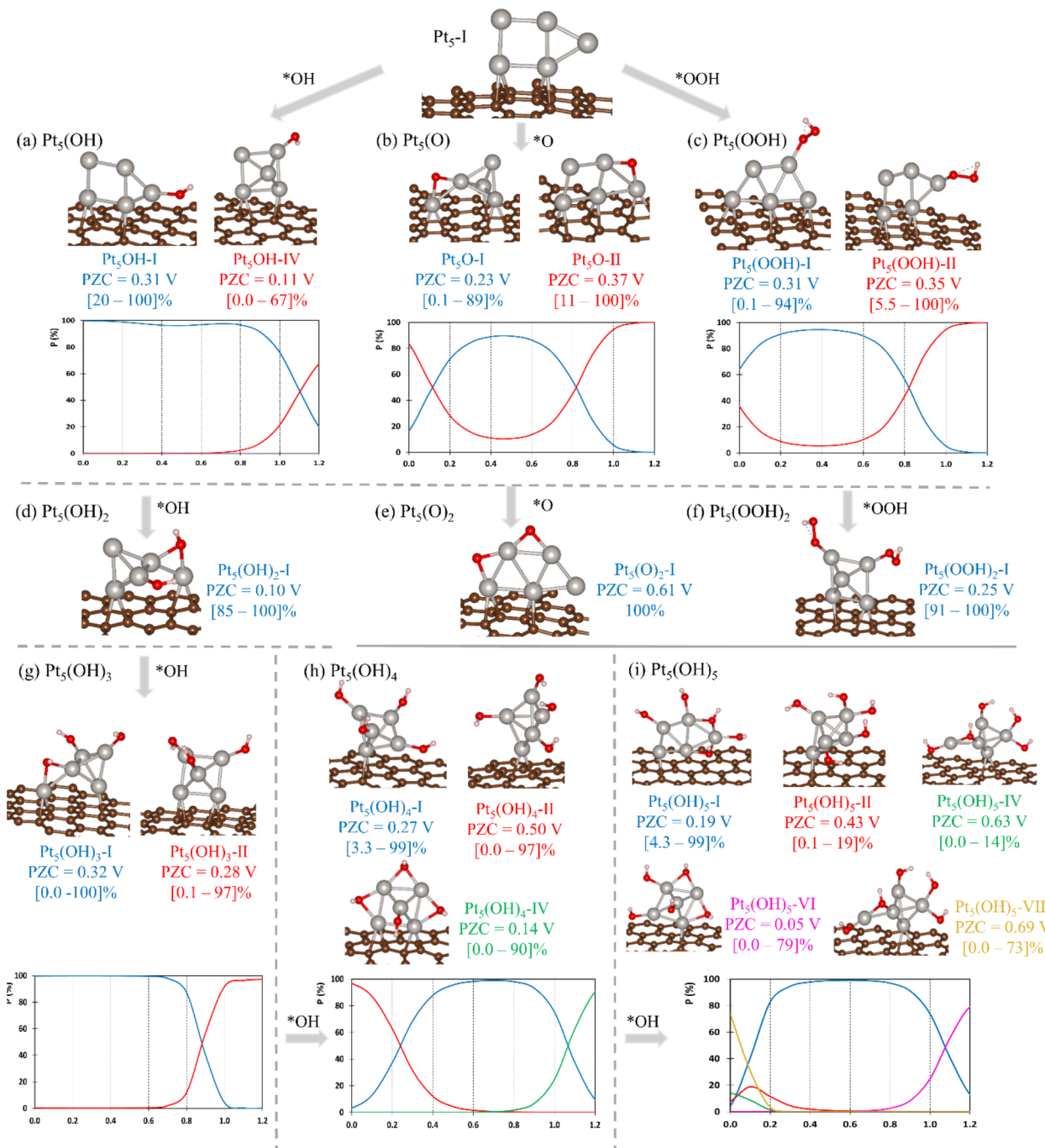


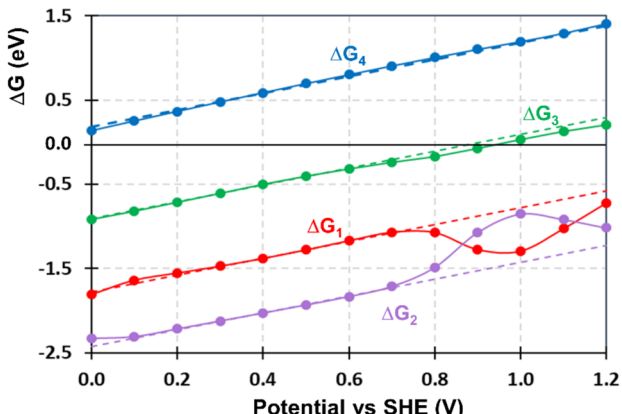
**Figure 2.** Selected local minima for  $\text{Pt}_5$ -adsorbate systems, PZC, and Boltzmann cluster distribution as a function of the potential in the SC framework at 300 K. The  $x$  axis corresponds to the potentials (vs SHE) in units of V.

alteration. The ensemble composition in the CHE picture would be 86% of  $\text{Pt}_5(\text{OH})_4\text{-I}$  and 13% of  $\text{Pt}_5(\text{OH})_4\text{-II}$  at all potentials at 300 K.

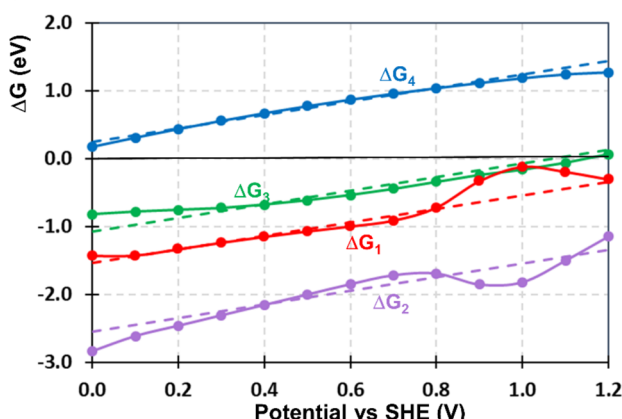
Finally,  $\text{Pt}_5(\text{OH})_5$  clusters also exhibit a strong geometric dependence on the applied potential (Figure 2i). Namely, in the 0.0–1.2 V range, there are three main predominant regions: 0.0–0.1, 0.1–1.0, and 1.0–1.2 V. Between 0 and 0.1 V,  $\text{Pt}_5(\text{OH})_5\text{-VIII}$  is the majority, with 73% of the population at 0 V. Other significant structures in this range are the GM for the neutral systems ( $\text{Pt}_5(\text{OH})_5\text{-I}$ ), as well as  $\text{Pt}_5(\text{OH})_5\text{-II}$  and  $\text{Pt}_5(\text{OH})_5\text{-VI}$ . Note that, while  $\text{Pt}_5(\text{OH})_5\text{-VIII}$  is 0.23 eV higher in energy than the GM, their PZC values are very different (0.19 V for  $\text{Pt}_5(\text{OH})_5\text{-I}$  and 0.69 V for  $\text{Pt}_5(\text{OH})_5\text{-VIII}$ , Figure 2i), which, in conjunction with a different curvature in the parabola is responsible for the switch in the potential-dependent GM (Figure S20). In addition, when inspecting Figure 2i, it is clear that  $\text{Pt}_5(\text{OH})_5\text{-VI}$  and  $\text{Pt}_5(\text{OH})_5\text{-VIII}$  show very similar geometries, only exhibiting subtle differences in interatomic distances. Namely, when considering the neutral systems,  $\text{Pt}_5(\text{OH})_5\text{-VI}$  is only 0.02 eV more stable than  $\text{Pt}_5(\text{OH})_5\text{-VIII}$ . This way, when including the potential effect via SC, the combination of PZC and parabola's curvature translates into  $\text{Pt}_5(\text{OH})_5\text{-VIII}$  being more stable in the considered potential range. Between 0.1 and 1.0 V,  $\text{Pt}_5(\text{OH})_5\text{-I}$  constitutes the majority, while at potentials above

VIII, Figure 2i), which, in conjunction with a different curvature in the parabola is responsible for the switch in the potential-dependent GM (Figure S20). In addition, when inspecting Figure 2i, it is clear that  $\text{Pt}_5(\text{OH})_5\text{-VI}$  and  $\text{Pt}_5(\text{OH})_5\text{-VIII}$  show very similar geometries, only exhibiting subtle differences in interatomic distances. Namely, when considering the neutral systems,  $\text{Pt}_5(\text{OH})_5\text{-VI}$  is only 0.02 eV more stable than  $\text{Pt}_5(\text{OH})_5\text{-VIII}$ . This way, when including the potential effect via SC, the combination of PZC and parabola's curvature translates into  $\text{Pt}_5(\text{OH})_5\text{-VIII}$  being more stable in the considered potential range. Between 0.1 and 1.0 V,  $\text{Pt}_5(\text{OH})_5\text{-I}$  constitutes the majority, while at potentials above

## (a) One adsorbate



## (b) Two adsorbates



## (c) 1–5 OH adsorbates

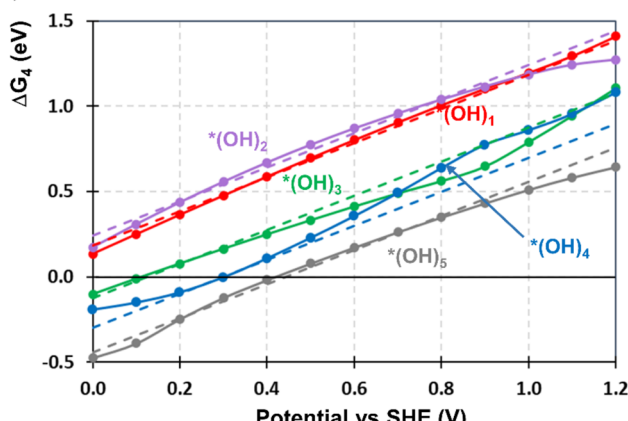


**Figure 3.**  $\Delta G$  for the four steps of the 4-e<sup>-</sup> mechanism of ORR of (a) Pt<sub>5</sub>/graphite with one adsorbate and (b) two adsorbates. (c)  $\Delta G_4$  ( $\Delta G$  for the fourth step of the 4-e<sup>-</sup> mechanism of ORR) of Pt<sub>5</sub>/graphite with 1–5 \*OH adsorbates. SC results are shown in solid lines and CHE ones in dotted lines.

1.0 V, Pt<sub>5</sub>(OH)<sub>5</sub>-VI does. This is mainly attributed to a sharper parabola curvature for Pt<sub>5</sub>(OH)<sub>5</sub>-VI (Figure S20).

The populations at 300 K derived from the CHE approach are 94% of Pt<sub>5</sub>(OH)<sub>5</sub>-I, 5% of Pt<sub>5</sub>(OH)<sub>5</sub>-II, 0.3% of Pt<sub>5</sub>(OH)<sub>5</sub>-III, and only 0.1% of other clusters, which reveals the large sensitivity of the ensemble composition of the adsorbate decorated electrocatalysts to the applied potential. One complication here is that with five adsorbates, we start finding

cluster geometries which are less bonded to the support. This might indicate the high propensity for sintering, affecting the practicability of ORR catalysis on Pt<sub>n</sub>/graphite.

**ORR Electrocatalysis on Pt<sub>5</sub>/Graphite.** We now explicitly address the energetics of the ORR steps, with the special focus on the potential-limiting reaction step (step 4 in Scheme 1). The following discussion is based on the system ensemble-averaged adsorption energies (Figure 3), but qualitatively similar conclusions can be drawn when the energies are computed with respect to the GM at each potential (see Figure S22). We first consider one adsorbate, ensemble binding energies of \*O, \*OH, and \*OOH ( $\Delta G_O$ ,  $\Delta G_{OH}$ , and  $\Delta G_{OOH}$ ) to Pt<sub>5</sub> being shown in the Supporting Information (Figure S21). \*OOH shows the least favorable binding, between 2.63 and 3.18 eV (versus 3.14 eV in the CHE framework). Notice that  $\Delta E_{OOH}$  exhibits a “shoulder” at about 0.8–1.2 V, due to the GM switching from Pt<sub>5</sub>(OOH)-I to Pt<sub>5</sub>(OOH)-II in this region, which affects the relative cluster proportions and thus the total ensemble energy of the system.  $\Delta G_O$  is in the range between 0.71 and 0.78 eV (versus 0.72 eV in the CHE framework). Remarkably,  $\Delta G_{OH}$  is negative, −0.18 eV in CHE, and between −0.13 and −0.21 eV in SC, revealing that Pt<sub>5</sub>/graphite suffers from overbinding, which is expected to limit the ORR activity and will lead to the catalytic interface being covered with \*OH adsorbates.<sup>25</sup>

Based on adsorption energies, we computed  $\Delta G$  for the four steps of ORR (Scheme 1,  $\Delta G_1$  to  $\Delta G_4$ ) as a function of the potential for the system covered by one and two adsorbates (Figure 3a and b), and  $\Delta G$  for the fourth step ( $\Delta G_4$ ) for 1–5 \*OH adsorbates (Figure 3c). As shown in Figure 3a for the case in which only one adsorbate is considered, due to \*OH overbinding,  $\Delta G_4$  (protonation of \*OH to produce water) is the thermodynamically limiting step of ORR, being positive in the entire potential range, 0–1.2 V.<sup>15,25,66</sup> This would suggest that Pt<sub>5</sub>/graphite is inactive toward ORR catalysis in the considered coverage conditions, as  $\Delta G_4$  becomes negative at about −0.1 V, which would correspond to an ORR overpotential higher than 1.23 V. This result resonates with previous calculations on Pt<sub>5</sub>, which, under an already explained different approach, predicted an overpotential of 1.04 V.<sup>15</sup>

When comparing SC and CHE approaches, significant differences between them are found. While they are almost indistinguishable in the low potential range, the GM switching in Pt<sub>5</sub>(OOH) translates into important oscillations in  $\Delta G_1$  and  $\Delta G_2$ , even leading to them crossing at 1.0 V. We note that relevant differences between the two approaches had also been proposed by some of us,<sup>61</sup> and other authors have also reported that explicit inclusion of the electrochemical potential in the calculation leads to potential-dependent differences in surface termination and reaction mechanisms.<sup>67–69</sup>

Next, we study how coverage affects the energetics of the reaction steps. We added an extra \*O, \*OH, and \*OOH adsorbate to the previous structures, i.e. \*OH to Pt<sub>5</sub>(OH), \*OOH to Pt<sub>5</sub>(OOH), and \*O to Pt<sub>5</sub>(O), and computed the binding energies (with regard to the previous coverage) and the derived  $\Delta G$  values for the four steps of ORR. We found that the absolute values of the binding energies are relatively similar to those computed for a single adsorbate (see Figure S21a and b). Unfortunately, the binding energy of \*OH is roughly the same (even about 0.05 eV more negative at low potentials) as for Pt<sub>5</sub>(OH), indicating that this coverage increase does not mitigate the overbinding, and ORR would not take place in the potential range between 0 and 1.23 V (as

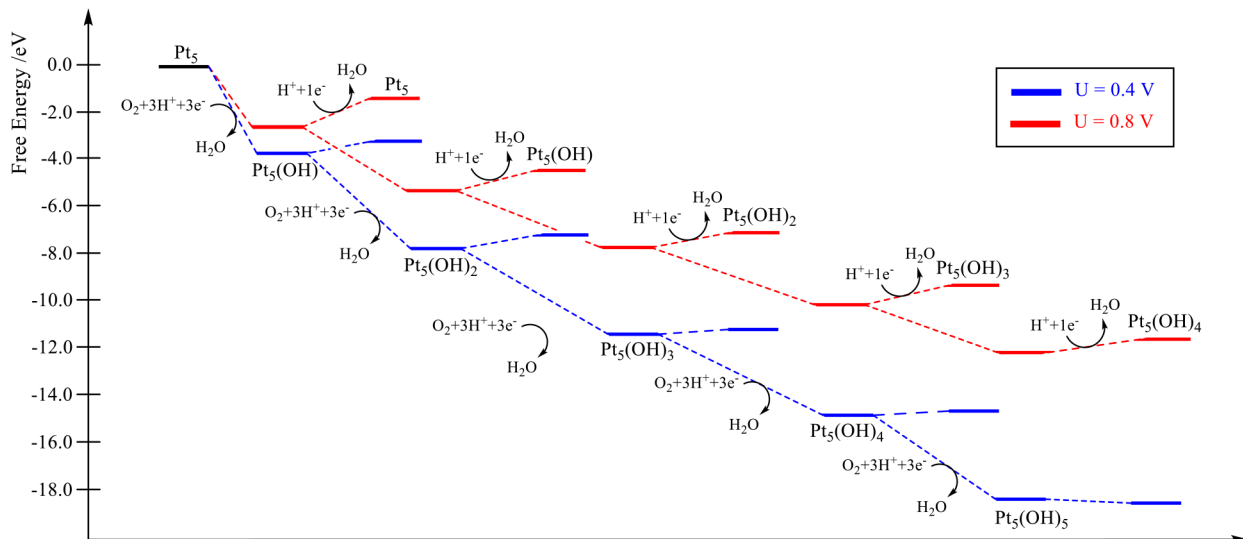


**Figure 4.** Free energy diagram for ORR and hydroxylation process of Pt<sub>5</sub>/graphite at potentials of 0.4 and 0.8 V (with regard to SHE). Steps 1–3 of ORR are represented together as Pt<sub>5</sub>(OH)<sub>n</sub> + O<sub>2</sub> + 3H<sup>+</sup> + 3e<sup>-</sup> → Pt<sub>5</sub>(OH)<sub>n+1</sub> + H<sub>2</sub>O.

ΔG<sub>4</sub> is positive, unfavorable in the whole range). Moreover, the negative adsorption energy for \*OH would strengthen the possibility of the real catalytic interface being covered by \*OH adsorbates.

Hence, as \*OH adsorption is by far more favorable than \*O and \*OOH, and the ORR thermodynamic-limiting reaction step is #4-\*OH protonation to yield water, we only consider further addition of \*OH to the cluster catalyst ensemble (Figure 3c). The third \*OH leads to a change in both the binding sites and the cluster shape, which is typical of sub-nano-cluster catalysis.<sup>65</sup> This has relevant implications for the energetics of the activity-limiting ORR step. Specifically, ΔG<sub>OH</sub> is now positive (about 0.2–0.4 eV increase compared to two adsorbates), indicative of partial mitigation of overbinding. This leads to ΔG<sub>4</sub> (intimately related to −ΔG<sub>OH</sub>, see Computational Details in the Supporting Information) being negative (favorable) at potentials lower than 0.1 V, which corresponds to an ORR overpotential of 1.12 V, in both CHE and SC approaches. Interestingly, the CHE and SC binding energies (and thus ΔG<sub>4</sub> values) are relatively similar at low potentials (between 0 and 0.3 V, and that is why they lead to similar overpotentials) but differ significantly at potentials higher than 0.3 V. This is a consequence of cluster fluxionality and the parabolic dependence of the system's Gibbs energy on the potential.

ORR energetics are even more favorable upon adsorption of the fourth \*OH, which leads to an additional change in the cluster morphology. ΔG<sub>OH</sub> increases at low potentials, while it is less unfavorable than that derived from three adsorbates at 0.7–1.2 V. Notice that ΔG<sub>OH</sub> in the SC framework deviates significantly from that derived from CHE (see Figure 3c). The increase in ΔG<sub>OH</sub> at low potentials leads to a further decrease in the ORR overpotential. Namely, the ORR onset potential—the potential at which all reaction steps became thermodynamically favorable—would be 0.30 V, corresponding to an overpotential of 0.93 V.

This favorable tendency holds for the fifth adsorbate, which further destabilizes \*OH adsorption by about 0.1–0.4 eV (depending on the potential, Figure 3c). The destabilization benefits the fourth ORR step, which now becomes exothermic

at 0.4 V; that is, the system would have an ORR overpotential of 0.81 V.

Thus, we can see that increasing cluster coverage reduced ORR overpotential, and although it keeps being higher than that of Pt(111) (about 0.4 V),<sup>32,70,71</sup> it is indicative of the activity increase. In addition, it should be highlighted that, even though the overpotential of these clusters is higher than that of Pt(111), the Pt loading in cluster systems is much lower, and the relative surface area and site-specificity to interact with O<sub>2</sub> molecules is higher, which can overcome the overpotential increase in practical applications.<sup>15,72</sup> Note that adsorption energies of \*OH point toward the adsorption of the first two adsorbates being thermodynamically favorable, thus revealing that the real catalytic interface will be covered by \*OH. In order to assess the potential competition between cluster hydroxylation and ORR, in Figure 4 we compare their relative energetics for U(SHE) of 0.4 and 0.8 V. The results show that cluster hydroxylation (i.e., steps 1 to 3 of ORR) is the preferred pathway, thus indicating that high cluster coverage is expected for these systems. The extent to which this coverage takes place would also depend on the experimental conditions such as electrolyte concentration (we are not explicitly considering the pH effect in this contribution) and temperature and is expected to hinder the system performance. Nevertheless, our results reveal how increasing coverage, coupled to cluster restructuring and surface charging, affects the catalytic activity and how all these effects need to be taken into account to find the actual active site.<sup>73</sup>

## CONCLUSIONS

This study reveals that an accurate description of cluster-decorated electrochemical interfaces requires explicit consideration of the electrochemical potential and the restructuring of the interface at this potential, and in the presence of the adsorbates at relevant coverages. Because of the highly fluxional character of supported sub-nano-clusters, they are able to change shapes as a function of the applied potential, so that the dominant species in the cluster population can also be highly potential-dependent. We expect the behavior to be non-monotonic with the Pt cluster size, as Pt<sub>3</sub> and Pt<sub>5</sub> behave differently, and the same happens with different adsorbate

coverages for Pt<sub>5</sub>: some systems show a more pronounced structural sensitivity to the potential. Moreover, the example of Pt<sub>5</sub> with adsorbates highlights the dramatic geometrical change that takes place when adsorbates bind to the clusters in their potential-dependent binding modes. Considering more relevant higher coverages is also evidently crucial for predicting the ORR activity, where at lower coverages, the \*OH adsorption is too strong and incompatible with the ORR activity. These results have important implications for cluster electrocatalysis, as they highlight the crucial effect of the applied potential on the ensemble composition, thus providing a step forward in the accurate modeling of fluxional electrochemical interfaces, and in the understanding of novel catalysts with switchable properties a function of the potential.

As a final comment, we should note that parameters in the model can affect the absolute values of binding energies and overpotentials. However, the results highlight important phenomena that must hold true regardless of the model, such as potential-dependent cluster fluxionality and interface restructuring, and, consequently, potential-dependent binding energies and ORR steps energetics (and thus overpotentials).

## ASSOCIATED CONTENT

### Supporting Information

The Supporting Information is available free of charge at <https://pubs.acs.org/doi/10.1021/acscatal.2c04643>.

Computational details of the calculations, local minima included in the ensembles and SC parabolic fittings, binding energies and ΔG for ORR steps ([PDF](#))

## AUTHOR INFORMATION

### Corresponding Authors

Anastassia N. Alexandrova — Department of Chemistry and Biochemistry, University of California, Los Angeles, Los Angeles, California 90095-1569, United States; California NanoSystem Institute, University of California, Los Angeles, Los Angeles, California 90095-1569, United States;  
✉ [orcid.org/0000-0002-3003-1911](https://orcid.org/0000-0002-3003-1911); Email: [ana@chem.ucla.edu](mailto:ana@chem.ucla.edu)

Philippe Sautet — Department of Chemistry and Biochemistry, University of California, Los Angeles, Los Angeles, California 90095-1569, United States; California NanoSystem Institute, University of California, Los Angeles, Los Angeles, California 90095-1569, United States; Department of Chemical and Biomolecular Engineering, University of California, Los Angeles, Los Angeles, California 90095, United States;  
✉ [orcid.org/0000-0002-8444-3348](https://orcid.org/0000-0002-8444-3348); Email: [sautet@ucla.edu](mailto:sautet@ucla.edu)

### Authors

Julen Munarriz — Department of Chemistry and Biochemistry, University of California, Los Angeles, Los Angeles, California 90095-1569, United States; Departamento de Química Física y Analítica, Universidad de Oviedo, Oviedo 33006, Spain;  
✉ [orcid.org/0000-0001-6089-6126](https://orcid.org/0000-0001-6089-6126)

Zisheng Zhang — Department of Chemistry and Biochemistry, University of California, Los Angeles, Los Angeles, California 90095-1569, United States

Complete contact information is available at:  
<https://pubs.acs.org/doi/10.1021/acscatal.2c04643>

## Funding

We acknowledge the support from the U.S. Department of Energy grant DE-SC0020125.

## Notes

The authors declare no competing financial interest.

## ACKNOWLEDGMENTS

The authors acknowledge the computational resources and technical assistance from NERSC, INCITE, and UCLA shared cluster, Hoffman2.

## REFERENCES

- (1) Chu, S.; Majumdar, A. Opportunities and challenges for a sustainable energy future. *Nature* **2012**, *488*, 294–303.
- (2) Mekhilef, S.; Saidur, R.; Safari, A. Comparative study of different fuel cell technologies. *Renew. Sustain. Energy Rev.* **2012**, *16*, 981–989.
- (3) Joya, K. S.; Joya, Y. F.; Ocakoglu, K.; van de Krol, R. Water-splitting catalysis and solar fuel devices: artificial leaves on the move. *Angew. Chem. Int. Ed.* **2013**, *52*, 10426–10437.
- (4) Lewis, N. S.; Nocera, D. G. Powering the planet: Chemical challenges in solar energy utilization. *Proc. Natl. Acad. Sci. U. S. A* **2006**, *103*, 15729–15735.
- (5) Halder, A.; Curtiss, L. A.; Fortunelli, A.; Vajda, S. Perspective: Size selected clusters for catalysis and electrochemistry. *J. Chem. Phys.* **2018**, *148*, 110901.
- (6) von Weber, A.; Anderson, S. L. Electrocatalysis by Mass-Selected Pt<sub>n</sub> Clusters. *Acc. Chem. Res.* **2016**, *49*, 2632–2639.
- (7) Seger, B.; Kamat, P. V. Electrocatalytically Active Graphene-Platinum Nanocomposites. Role of 2-D Carbon Support in PEM Fuel Cells. *J. Phys. Chem. C* **2009**, *113*, 7990–7995.
- (8) Kou, R.; Shao, Y.; Wang, D.; Engelhard, M. H.; Kwak, J. H.; Wang, J.; Viswanathan, V. V.; Wang, C.; Lin, Y.; Wang, Y.; Aksay, I. A.; Liu, J. Enhanced activity and stability of Pt catalysts on functionalized graphene sheets for electrocatalytic oxygen reduction. *Electrochim. Commun.* **2009**, *11*, 954–957.
- (9) Zhang, B.-W.; Ren, L.; Xu, Z.-F.; Cheng, N.-Y.; Lai, W.-H.; Zhang, L.; Hao, W.; Chu, S.-Q.; Wang, Y.-X.; Du, Y.; Jiang, L.; Liu, H.-K.; Dou, S.-X. Atomic Structural Evolution of Single-Layer Pt Clusters as Efficient Electrocatalysts. *Small* **2021**, *17*, 2100732.
- (10) Inaba, M.; Zana, A.; Quinson, J.; Bizzotto, F.; Dosche, C.; Dworzak, A.; Oezaslan, M.; Simonsen, S. B.; Kuhn, L. T.; Arenz, M. The Oxygen Reduction Reaction on Pt: Why Particle Size and Interparticle Distance Matter. *ACS Catal.* **2021**, *11*, 7144–7153.
- (11) Proch, S.; Wirth, M.; White, H. S.; Anderson, S. L. Strong Effects of Cluster Size and Air Exposure on Oxygen Reduction and Carbon Oxidation Electrocatalysis by Size-Selected Pt<sub>n</sub> ( $n \leq 11$ ) on Glassy Carbon Electrodes. *J. Am. Chem. Soc.* **2013**, *135*, 3073–3086.
- (12) von Weber, A.; Baxter, E. T.; Proch, S.; Kane, M. D.; Rosenfelder, M.; White, H. S.; Anderson, S. L. Size-Dependent Electronic Structure Controls Activity for Ethanol Electro-Oxidation at Pt<sub>n</sub>/Indium Tin Oxide ( $n = 1$  to 14). *Phys. Chem. Chem. Phys.* **2015**, *17*, 17601–17610.
- (13) von Weber, A.; Baxter, E. T.; White, H. S.; Anderson, S. L. Cluster Size Controls Branching Between Water And Hydrogen Peroxide Production In Electrochemical Oxygen Reduction at Pt<sub>n</sub>/ITO. *J. Phys. Chem. C* **2015**, *119*, 11160–11170.
- (14) Magee, J. W.; Zhou, W.-P.; White, M. G. Promotion of Pt surfaces for ethanol electro-oxidation by the addition of small SnO<sub>2</sub> nanoparticles: Activity and mechanism. *Appl. Catal. B-Environ.* **2014**, *152–153*, 397–402.
- (15) Ohnuma, A.; Takahashi, K.; Tsunoyama, H.; Inoue, T.; Zhao, P.; Velloth, A.; Ehara, M.; Ichikuni, N.; Tabuchi, M.; Nakajima, A. Enhanced oxygen reduction activity of size-selected platinum subnanocluster catalysts: Pt<sub>n</sub> ( $n = 3$ –9). *Catal. Sci. Technol.* **2022**, *12*, 1400–1407.

- (16) Zandkarimi, B.; Alexandrova, A. N. Dynamics of Subnanometer Pt Clusters Can Break the Scaling Relationships in Catalysis. *J. Phys. Chem. Lett.* **2019**, *10*, 460–467.
- (17) Pérez-Ramírez, J.; López, N. Strategies to break linear scaling relationships. *Nat. Catal.* **2019**, *2*, 971–976.
- (18) Huang, Z.-F.; Song, J.; Dou, S.; Li, X.; Wang, J.; Wang, X. Strategies to Break the Scaling Relation toward Enhanced Oxygen Electrocatalysis. *Matter* **2019**, *1*, 1494–1518.
- (19) Opalka, D.; Scheurer, C.; Reuter, K. Ab Initio Thermodynamics Insight into the Structural Evolution of Working  $\text{IrO}_2$  Catalysts in Proton-Exchange Membrane Electrolyzers. *ACS Catal.* **2019**, *9*, 4944–4950.
- (20) Yoon, A.; Poon, J.; Grosse, P.; Chee, S. W.; Cuenya, B. R. Iodide-mediated Cu Catalyst Restructuring during  $\text{CO}_2$  Electro-reduction. *J. Mater. Chem. A* **2022**, *10*, 14041–14050.
- (21) Steinmann, S. N.; Sautet, P. Assessing a First-Principles Model of an Electrochemical Interface by Comparison with Experiment. *J. Phys. Chem. C* **2016**, *120*, 5619–5623.
- (22) Steinmann, S. N.; Michel, C.; Schwiedernoch, R.; Sautet, P. Impacts of electrode potentials and solvents on the electroreduction of  $\text{CO}_2$ : a comparison of theoretical approaches. *Phys. Chem. Chem. Phys.* **2015**, *17*, 13949–13963.
- (23) Liu, L.; Liu, C. Origin of the overpotentials for  $\text{HCOO}^-$  and CO formation in the electroreduction of  $\text{CO}_2$  on Cu(211): the reductive de-sorption processes decide. *Phys. Chem. Chem. Phys.* **2018**, *20*, 5756–5765.
- (24) Baxter, E. T.; Ha, M.-A.; Cass, A. C.; Alexandrova, A. N.; Anderson, S. L. Ethylene Dehydrogenation on  $\text{Pt}_{4,7,8}$  clusters on  $\text{Al}_2\text{O}_3$ : Strong Cluster-Size Dependence Linked to Preferred Catalyst Morphologies. *ACS Catal.* **2017**, *7*, 3322–3335.
- (25) Zhang, Z.; Zandkarimi, B.; Munarriz, J.; Dickerson, C. E.; Alexandrova, A. N. Fluxionality of Subnano Clusters Reshapes the Activity Volcano of Electrocatalysis. *ChemCatChem.* **2022**, *14*, No. e202200345.
- (26) Ramos-Sánchez, G.; Balbuena, P. B. Interactions of platinum clusters with a graphite substrate. *Phys. Chem. Chem. Phys.* **2013**, *15*, 11950–11959.
- (27) Lim, D.-H.; Wilcox, J. DFT-Based Study on Oxygen Adsorption on Defective Graphene-Supported Pt Nanoparticles. *J. Phys. Chem. C* **2011**, *115*, 22742–22747.
- (28) Okamoto, Y. Density-functional calculations of icosahedral  $\text{M}_{13}$  ( $\text{M} = \text{Pt}$  and  $\text{Au}$ ) clusters on graphene sheets and flakes. *Chem. Phys. Lett.* **2006**, *420*, 382–386.
- (29) Qi, Q.; Liu, H.; Feng, W.; Tian, H.; Xu, H.; Huang, X. Theoretical investigation on the interaction of subnano platinum clusters with graphene using DFT methods. *Comput. Mater. Sci.* **2015**, *96*, 268–276.
- (30) Ma, J.; Habrioux, A.; Luo, Y.; Ramos-Sánchez, G.; Calvillo, L.; Granozzi, G.; Balbuena, P. B.; Alonso-Vante, N. Electronic interaction between platinum nanoparticles and nitrogen-doped reduced graphene oxide: effect on the oxygen reduction reaction. *J. Mater. Chem. A* **2015**, *3*, 11891–11904.
- (31) Tsunoyama, H.; Ohnuma, A.; Takahashi, K.; Velloth, A.; Ehara, M.; Ichikuni, N.; Tabuchi, M.; Nakajima, A. Enhanced oxygen reduction activity of platinum subnanocluster catalysts through charge redistribution. *Chem. Commun.* **2019**, *55*, 12603–12606.
- (32) Nørskov, J. K.; Rossmeisl, J.; Logadottir, A.; Lindqvist, L.; Kitchin, J. R.; Bligaard, T.; Jónsson, H. Origin of the Overpotential for Oxygen Reduction at a Fuel-Cell Cathode. *J. Phys. Chem. B* **2004**, *108*, 17886–17892.
- (33) Kristoffersen, H. H.; Vegge, T.; Hansen, H. A. OH formation and  $\text{H}_2$  adsorption at the liquid water– $\text{Pt}(111)$  interface. *Chem. Sci.* **2018**, *9*, 6912–6921.
- (34) Mathew, K.; Sundararaman, R.; Letchworth-Weaver, K.; Arias, T. A.; Hennig, R. G. Implicit solvation model for density-functional study of nanocrystal surfaces and reaction pathways. *J. Chem. Phys.* **2014**, *140*, 084106.
- (35) Chang, K.; Zhang, H.; Chen, J. G.; Lu, Q.; Cheng, M.-J. Constant Electrode Potential Quantum Mechanical Study of  $\text{CO}_2$  Electrochemical Reduction Catalyzed by N-Doped Graphene. *ACS Catal.* **2019**, *9*, 8197–8207.
- (36) Goodpaster, J. D.; Bell, A. T.; Head-Gordon, M. Identification of Possible Pathways for C–C Bond Formation during Electrochemical Reduction of  $\text{CO}_2$ : New Theoretical Insights from an Improved Electrochemical Model. *J. Phys. Chem. Lett.* **2016**, *7*, 1471–1477.
- (37) Melander, M. M.; Kuisma, M. J.; Christensen, T. E. K.; Honkala, K. Grand-canonical approach to density functional theory of electrocatalytic systems: Thermodynamics of solid-liquid interfaces at constant ion and electrode potentials. *J. Chem. Phys.* **2019**, *150*, 041706.
- (38) Hutchison, P.; Rice, P. S.; Warburton, R. E.; Raugei, S.; Hammes-Schiffer, S. Multilevel Computational Studies Reveal the Importance of Axial Ligand for Oxygen Reduction Reaction on Fe–N–C Materials. *J. Am. Chem. Soc.* **2022**, *144*, 16524–16534.
- (39) Sundararaman, R.; Goddard, W. A., III; Arias, T. A. Grand canonical electronic density-functional theory: Algorithms and applications to electrochemistry. *J. Chem. Phys.* **2017**, *146*, 114104.
- (40) Smidstrup, S.; Stradi, D.; Wellendorff, J.; Khomyakov, P. A.; Vej-Hansen, U. G.; Lee, M.-E.; Ghosh, T.; Jónsson, E.; Jónsson, H.; Stokbro, K. First-principles Green's-function method for surface calculations: A pseudopotential localized basis set approach. *Phys. Rev. B* **2017**, *96*, 195309.
- (41) Bonnet, N.; Morishita, T.; Sugino, O.; Otani, M. First-Principles Molecular Dynamics at a Constant Electrode Potential. *Phys. Rev. Lett.* **2012**, *109*, 266101.
- (42) Nishihara, S.; Otani, M. Hybrid solvation models for bulk, interface, and membrane: Reference interaction site methods coupled with density functional theory. *Phys. Rev. B* **2017**, *96*, 115429.
- (43) Basdogan, Y.; Maldonado, A. M.; Keith, J. A. Advances and challenges in modeling solvated reaction mechanisms for renewable fuels and chemicals. *WIREs Comput. Mol. Sci.* **2020**, *10*, No. e1446.
- (44) Gauthier, J. A.; Ringe, S.; Dickens, C. F.; Garza, A. J.; Bell, A. T.; Head-Gordon, M.; Nørskov, J. K.; Chan, K. Challenges in Modeling Electrochemical Reaction Energetics with Polarizable Continuum Models. *ACS Catal.* **2019**, *9*, 920–931.
- (45) Abidi, N.; Lim, K. R. G.; Seh, Z. W.; Steinmann, S. N. Atomistic modeling of electrocatalysis: Are we there yet? *WIREs Comput. Mol. Sci.* **2021**, *11*, No. e1499.
- (46) Campos-Roldán, C. A.; Ramos-Sánchez, G.; Gonzalez-Huerta, R. G.; Vargas García, J. R.; Balbuena, P. B.; Alonso-Vante, N. Influence of  $\text{sp}^3$ – $\text{sp}^2$  Carbon Nanodomains on Metal/Support Interaction, Catalyst Durability, and Catalytic Activity for the Oxygen Reduction Reaction. *ACS Appl. Mater. Interfaces* **2016**, *8*, 23260–23269.
- (47) Yang, J.; Kim, S. H.; Kwak, S. K.; Song, H. – K. Curvature-Induced Metal–Support Interaction of an Islands-by-Islands Composite of Platinum Catalyst and Carbon Nano-onion for Durable Oxygen Reduction. *ACS Appl. Mater. Interfaces* **2017**, *9*, 23302–23308.
- (48) Schneider, W. B.; Benedikt, U.; Auer, A. A. Interaction of platinum nanoparticles with graphitic carbon structures: A computational study. *ChemPhysChem* **2013**, *14*, 2984–2989.
- (49) Poidevin, C.; Paciok, P.; Heggen, M.; Auer, A. A. High resolution transmission electron microscopy and electronic structure theory investigation of platinum nanoparticles on carbon black. *J. Chem. Phys.* **2019**, *150*, 041705.
- (50) Jayabal, S.; Saranya, G.; Geng, D.; Lin, L. Y.; Meng, X. Insight into the correlation of Pt–support interactions with electrocatalytic activity and durability in fuel cells. *J. Mater. Chem. A* **2020**, *8*, 9420–9446.
- (51) Duan, Z.; Henkelman, G. Atomic-Scale Mechanisms of Electrochemical Pt Dissolution. *ACS Catal.* **2021**, *11*, 14439–14447.
- (52) Zandkarimi, B.; Poths, P.; Alexandrova, A. N. When Fluxionality Beats Size Selection: Acceleration of Ostwald Ripening of Sub-Nano Clusters. *Angew. Chem. Int. Ed.* **2021**, *60*, 11973–11982.
- (53) Hu, X.; Chen, S.; Chen, L.; Tian, Y.; Yao, S.; Lu, Z.; Zhang, X.; Zhou, Z. What is the Real Origin of the Activity of Fe–N–C

Electrocatalysts in the O<sub>2</sub> Reduction Reaction? Critical Roles of Coordinating Pyrrolic N and Axially Adsorbing Species. *J. Am. Chem. Soc.* **2022**, *144*, 18144–18152.

(54) Zhai, H.; Alexandrova, A. N. Ensemble-Average Representation of Pt Clusters in Conditions of Catalysis Accessed through GPU Accelerated Deep Neural Network Fitting Global Optimization. *J. Chem. Theory Comput.* **2016**, *12*, 6213–6226.

(55) Peremans, A.; Tadjeddine, A. Electrochemical deposition of hydrogen on platinum single crystals studied by infrared-visible sum-frequency generation. *J. Chem. Phys.* **1995**, *103*, 7197–7203.

(56) Łosiewicz, B.; Jurczakowski, R.; Lasia, A. Kinetics of hydrogen underpotential deposition at polycrystalline platinum in acidic solutions. *Electrochim. Acta* **2012**, *80*, 292–301.

(57) Groves, M. N.; Malardier-Jugroot, C.; Jugroot, M. Improving Platinum Catalyst Durability with a Doped Graphene Support. *J. Phys. Chem. C* **2012**, *116*, 10548–10556.

(58) Zhai, H.; Alexandrova, A. N. Local Fluxionality of Surface-Deposited Cluster Catalysts: the Case of Pt<sub>7</sub> on Al<sub>2</sub>O<sub>3</sub>. *J. Phys. Chem. Lett.* **2018**, *9*, 1696–1702.

(59) Imaoka, T.; Toyonaga, T.; Morita, M.; Haruta, N.; Yamamoto, K. Isomerizations of a Pt<sub>4</sub> cluster revealed by spatiotemporal microscopic analysis. *Chem. Commun.* **2019**, *55*, 4753–4756.

(60) Shen, L.; Dadras, J.; Alexandrova, A. N. Pure and Zn-doped Pt clusters go flat and upright on MgO(100). *Phys. Chem. Chem. Phys.* **2014**, *16*, 26436–26442.

(61) Shang, R.; Steinmann, S. N.; Xu, B.-Q.; Sautet, P. Mononuclear Fe in N-doped carbon: computational elucidation of active sites for electrochemical oxygen reduction and oxygen evolution reactions. *Catal. Sci. Technol.* **2020**, *10*, 1006–1014.

(62) Zhang, Z.; Zandkarimi, B.; Alexandrova, A. N. Ensembles of metastable states govern heterogeneous catalysis on dynamic interfaces. *Acc. Chem. Res.* **2020**, *53*, 447–458.

(63) Zhai, H.; Alexandrova, A. N. Fluxionality of Catalytic Clusters: When It Matters and How to Address It. *ACS Catal.* **2017**, *7*, 1905–1911.

(64) Zhang, Z.; Cui, Z.-H.; Jimenez-Izal, E.; Sautet, P.; Alexandrova, A. N. Hydrogen Evolution on Restructured B-Rich WB: Metastable Surface States and Isolated Active Sites. *ACS Catal.* **2020**, *10*, 13867–13877.

(65) Lavroff, R. H.; Morgan, H. W. T.; Zhang, Z.; Poths, P.; Alexandrova, A. N. Ensemble representation of catalytic interfaces: soloists, orchestras, and everything in-between. *Chem. Sci.* **2022**, *13*, 8003–8016.

(66) Hansen, H. A.; Viswanathan, V.; Nørskov, J. K. Unifying Kinetic and Thermodynamic Analysis of 2 e<sup>-</sup> and 4 e<sup>-</sup> Reduction of Oxygen on Metal Surfaces. *J. Phys. Chem. C* **2014**, *118*, 6706–6718.

(67) Benedikt, U.; Schneider, W. B.; Auer, A. A. Modelling electrified interfaces in quantum chemistry: constant charge vs. constant potential. *Phys. Chem. Chem. Phys.* **2013**, *15*, 2712–2724.

(68) Ping, Y.; Nielsen, R. J.; Goddard, W. A., III The Reaction Mechanism with Free Energy Barriers at Constant Potentials for the Oxygen Evolution Reaction at the IrO<sub>2</sub> (110) Surface. *J. Am. Chem. Soc.* **2017**, *139*, 149–155.

(69) Yang, J. A computational study on the electrified Pt(111) surface by the cluster model. *Phys. Chem. Chem. Phys.* **2019**, *21*, 6112–6125.

(70) Hoogers, G.; Thompsett, D. The role of catalysis in proton exchange membrane fuel cell technology. *CATTECH* **1999**, *3*, 106.

(71) Kulkarni, A.; Siahrostami, S.; Patel, A.; Nørskov, J. K. Understanding Catalytic Activity Trends in the Oxygen Reduction Reaction. *Chem. Rev.* **2018**, *118*, 2302–2312.

(72) Debe, M. K. Electrocatalyst approaches and challenges for automotive fuel cells. *Nature* **2012**, *486*, 43–51.

(73) Pt<sub>5</sub> clusters over glassy carbon have been found to be active towards ORR, as described in reference 15.

## □ Recommended by ACS

### Activity Enhancement of PtIr Catalysts for Complete Ethanol Oxidation Reaction by Tuning C–O Coupling Abilities

Ruitao Wu and Lichang Wang

DECEMBER 14, 2022

THE JOURNAL OF PHYSICAL CHEMISTRY C

READ ▶

### Does the Encapsulation Strategy of Pt Nanoparticles with Carbon Layers Really Ensure Both Highly Active and Durable Electrocatalysis in Fuel Cells?

Sang Gu Ji, Chang Hyuck Choi, et al.

JUNE 03, 2022

ACS CATALYSIS

READ ▶

### Optimizing the Electronic Structure of Ordered Pt–Co–Ti Ternary Intermetallic Catalyst to Boost Acidic Oxygen Reduction

Weiyu Zhao, Shijun Liao, et al.

JUNE 13, 2022

ACS CATALYSIS

READ ▶

### Synergistic Hybrid Electrocatalysts of Platinum Alloy and Single-Atom Platinum for an Efficient and Durable Oxygen Reduction Reaction

Bowen Liu, Qinglei Liu, et al.

AUGUST 26, 2022

ACS NANO

READ ▶

Get More Suggestions >